PERGAMON

Journal of Structural Geology 22 (2000) 453–469

JOURNAL OF STRUCTURAL GEOLOGY

www.elsevier.nl/locate/jstrugeo

Tectonics of the circum-Troodos sedimentary cover of Cyprus, from rock magnetic and structural observations

France Lagroix, Graham J. Borradaile*

Geology Department, Lakehead University, Thunder Bay, Canada P7B 5E1

Received 9 June 1999; accepted 2 November 1999

Abstract

The calcareous sedimentary cover of the Troodos Ophiolite Complex dips gently away from the Troodos Complex. It has rare, usually open folds and, locally, stylolitic cleavage (S_1). Stylolitic cleavage is ~50% more effective than primary bedding-stylolites in removing matrix and the variation in the S_1 vergence directions are compatible with gravitational sliding radially away from the Troodos range and into sedimentary basins. Two different types of magnetic fabric, anisotropy of magnetic susceptibility (AMS) and anisotropy anhysteretic remanence (AARM), reveal the sequence of preferred orientations of different minerals, and the vergence of their magnetic foliations with respect to bedding reveals the sense of over-shearing of the stratigraphic sequence. AMS defines crystallographic alignments of clay minerals and dimensional alignments of magnetite in the limestones. AARM isolates the preferred dimensional orientation of magnetite. Although traces of magnetite dominate the *bulk* susceptibility, its anisotropy is low in comparison with phyllosilicates so that AMS essentially records the clay-fabric. Throughout the study area, AMS foliation indicates *S*-vergence and AMS lineation indicates N–S extension. AMS foliation-vergence indicates shearing of the entire sedimentary cover southward from Troodos. This motion is attributed to gravity sliding controlled by regional uplift to the north. In contrast, AARM foliation indicates a subsequent ESE vergence due to later WNW–ESE extension. The NNE, AARM lineation is a composite of bedding and tectonic fabric contributions that do not directly yield a faithful extension direction. The shapes of the magnetic fabrics indicate that AMS (clay) fabrics have a broad range of shapes about the neutral ellipsoid shape, whereas AARM (magnetite) fabrics are bimodal, with equally developed bedding-oblate and tectonic linear–planar ($L = S$) components. Hysteresis properties, plotted on a new three-dimensional diagram, show clearly that the magnetite has a pseudosingle domain response, so there is no reason to expect complications from inverse fabrics due to single-domain magnetite. Moreover it shows that hysteresis properties vary systematically with depositional depth, reflecting systematic changes in magnetite granulometry with sedimentary environment.

1. Introduction

Cyprus occupies a unique position in the Eastern Mediterranean, providing key information on the evolution of Tethys and microplate motion in that region from its four geological and tectonic elements (Figs. 1a and 2). During the Permian, shallow water limestones accumulated on the northward dipping shelf of Gondwanaland, now exposed in the Kyrenia Terrain (Fig. 3). Triassic rifting of the northern margin of Gondwana may have separated the Kyrenia terrain; it certainly isolated rocks of the Mamonia terrain on the edge of a microcontinent (Robertson, 1990; Fig. 3). Through the Jurassic and Early Cretaceous the southern or Neo-Tethyan Ocean opened continuously, accompanied by a subordinate eastward motion of the African continent with respect to Eurasia. During the Mid-Cretaceous (~119 Ma), the African plate veered northward (Dewey et al., 1973; Dilek et al., 1990) initiating subduction in the region of Cyprus (Fig. 3a). By the late Cretaceous the Troodos terrain was located in a supra-subduction sequence and the terrains that now

* Corresponding author.
E-mail address: borradaile@lakeheadu.ca (G.J. Borradaile).

0191-8141/00/$ - see front matter
PII: S0191-8141(99)00168-6

comprise Cyprus began to rotate counterclockwise (Fig. 3d); by the Paleocene about 60° rotation was complete and subduction had ceased on the present south side of Troodos (Eaton and Robertson, 1993; Fig. 3b). By the Miocene, subduction was reinitiated on the present day Cyprean arc (Fig. 3c). In the reconstructions of Fig. 3, it is important to note that *present day* north and south are shown in all cases; the actual orientation of the terrains was inferred paleomagnetically and is summarized in Fig. 3(d) (Clube and Robertson, 1986). In the late Pliocene all terrains united and emerged (Robertson, 1977; Robertson and Woodcock, 1979, 1986).

Cyprus is renowned for its well-exposed ophiolite sequence, in the Troodos Mountains. A mantle sequence of harzburgite–lhertzolite is overlain by a

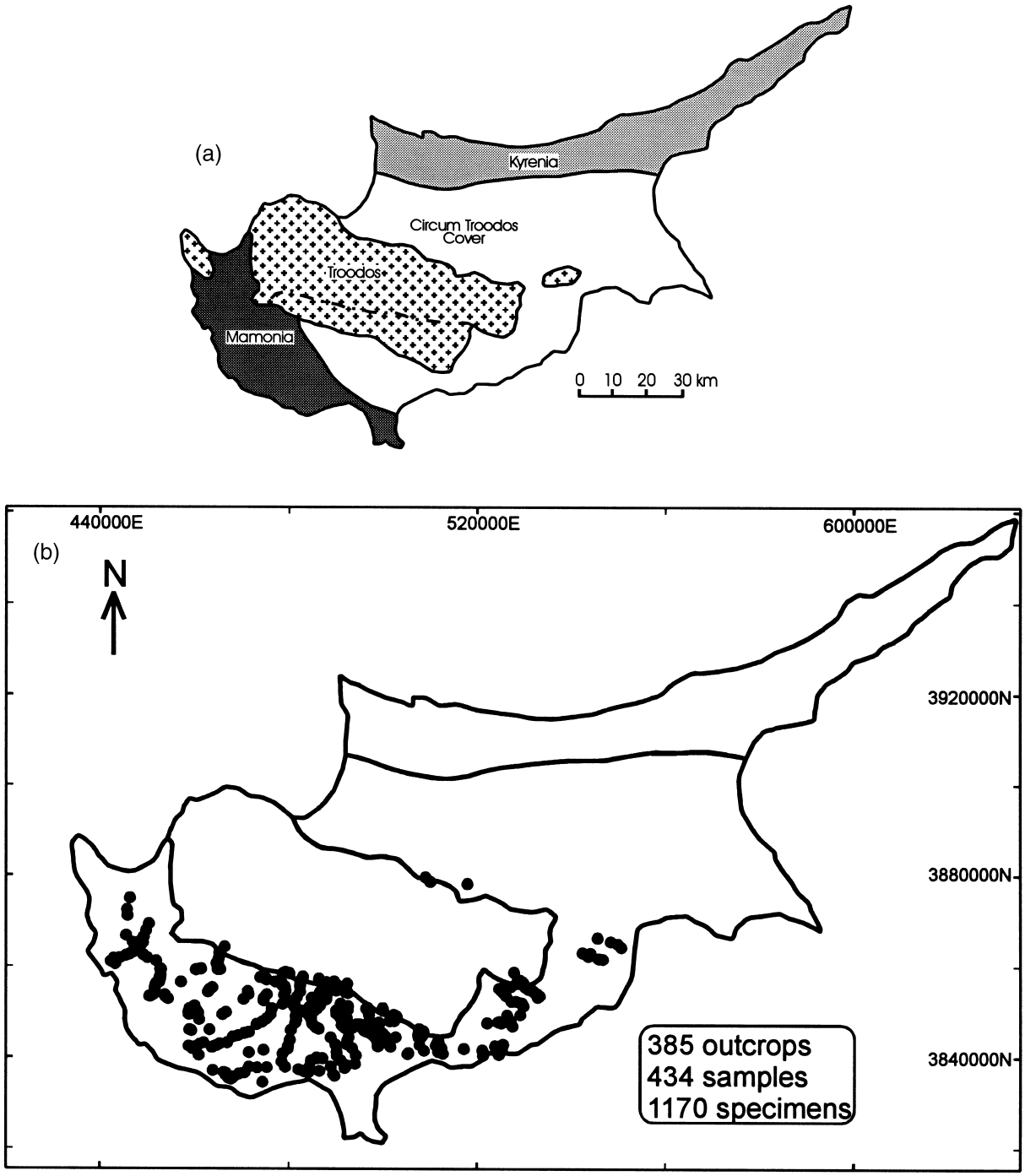

Fig. 1. (a) The four main geological regions of Cyprus. (b) The outcrop location map of the study area. Dots indicate outcrop locations.

complex of (now) N–S dikes that indicates the original ocean floor spreading direction, although the ophiolite sequence has since been rotated 90° anticlockwise (Fig. 3d). It is succeeded by pillow lava, and then a pelagic, but gradually shallowing, limestone sequence. The ophiolite sequence started to form ~90 Ma ago according to radiolarian biostratigraphy (Blowe and Irwin, 1985) and from U–Pb ages of plagiogranite in the Troodos mantle sequence (Musaka and Ludden, 1987). The Troodos terrain was formed within 20 km of a spreading axis, in a supra-subduction setting between two trenches (Fig. 3a). The chalks immediately overlying the pillow lava sequence reveal a progressive rotation of the Troodos microplate of 90° anticlockwise over 25 Ma, from the Late Cretaceous to the Early Eocene from paleomagnetic studies (Clube and Robertson, 1986). Also, by the Eocene, the Mamonia and Troodos terrains docked, both being overlain by the Lefkara Limestones (74–24 Ma; Robertson and Woodcock, 1979; Fig. 3b).

The ocean basin to the north closed during the Pliocene, and in the Pleistocene the three terrains and its sedimentary cover were uplifted on a regional scale, the effects of uplift being recorded 250 km offshore east of Cyprus (McCallum and Robertson, 1990). However, localized uplift at the centre of the Troodos ophiolite terrain was severe and radial (Robertson, 1977). It is attributed to dilational uplift by serpentinization, superimposed on the regional compression (Robertson, 1990).

2. This study

We have focused on the microstructural features of the limestone cover sequence in order to determine the roles of compression and uplift in the late tectonic evolution of Cyprus, and in particular on events related to uplift of the Troodos terrain. Our information derives from the stratigraphic sequence overlying the ophiolite, comprising the upwards-shallowing limestone formations: Lefkara (74–24 Ma), Pakhna (24–8 Ma) and Nicosia (8–5 Ma). We will provide evidence concerning the bedding, cleavage, and two asynchronous magnetic fabrics in the circum-Troodos cover. The data have been analyzed in different subareas, but for the purposes of ease of representation, which does not change the interpretation, we chose six *regularly-shaped* rectangular subareas fringing the SW, S and SE margins of the Troodos terrain.

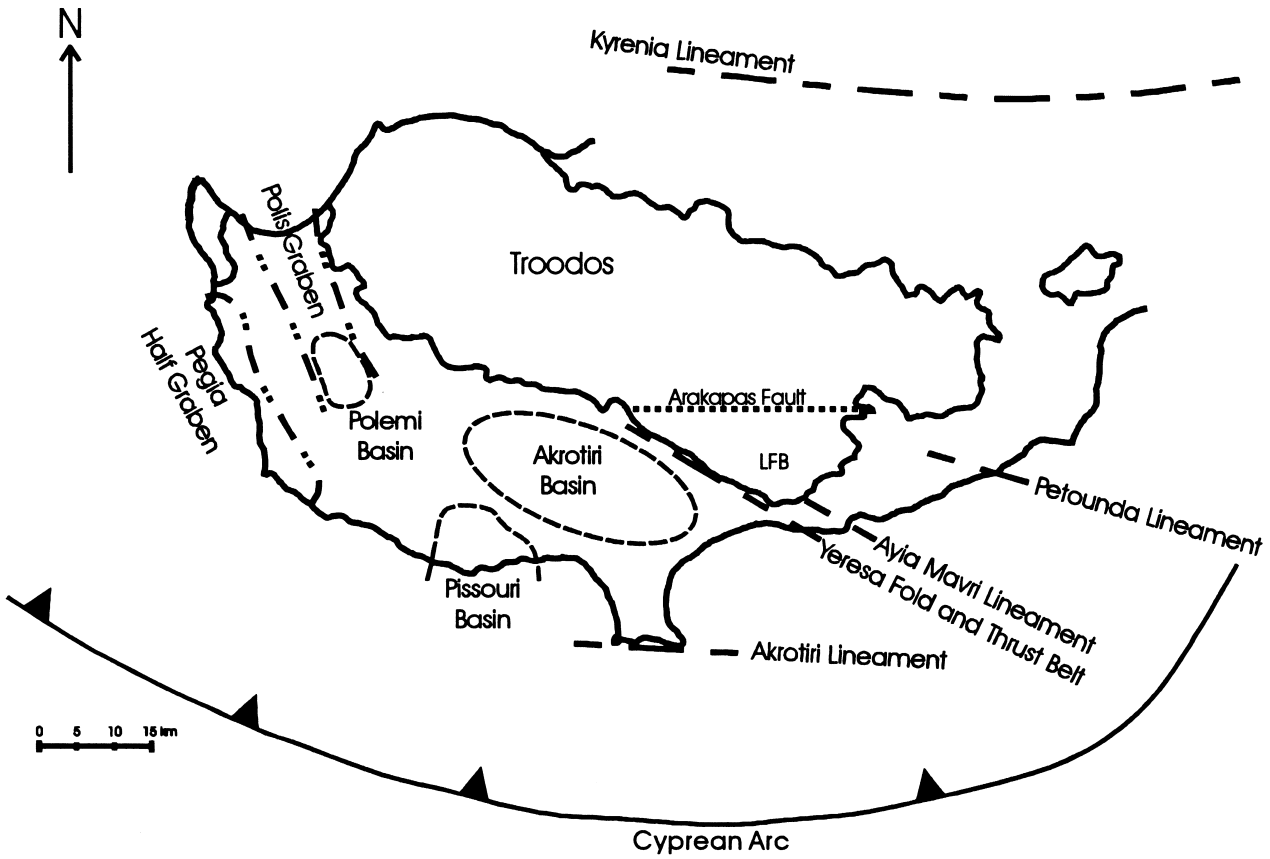

Fig. 2. Principal tectonic elements of Cyprus.

With the exception of very small, localized areas, less than a few kilometres in dimensions, the largest of which is the Yeresa fold and thrust belt, near Limassol (Fig. 2), distinctive tectonic folds are absent. Rock cleavage is however well developed and is of the stylolitic spaced type. This is nevertheless axial planar to small folds and to the rare, usually open larger folds. Bedding is little disturbed so that cleavage stylolites are distinguished easily from bedding stylolites. Cleavage stylolites are generally 50% thicker than bedding stylolites and clearly offset bedding (Fig. 4). They attest to extensive pressure solution in the pelagic sequence during its deformation after bedding-stylolitization and at a more indurated point in its history. The extensive removal of carbonate that formed S_1 makes it easy to understand the penetrative nature of reorientation of mineral grains that are detected by magnetic fabric methods, below.

Fig. 5 shows the orientations of bedding and S_1 in each subarea. The bedding-poles cluster strongly, indicating the gentle dips, radially away from the Troodos Mountains of central Cyprus. The S_1-poles are less convincingly clustered for two reasons. First, S_1 is only locally developed and relatively few observations are possible. Secondly, it is by nature a rough cleavage, with poor directional stability. Subsequently, however, we will show that the vergence of S_1, determined from the *local* angular relations of S_1 with respect to bedding, are consistent within each subarea, but different between subareas.

Thus, conventional field structures yield relatively little information on the penetrative deformation of the sedimentary cover, which is of interest to us in understanding the kinematics of regional deformation. Structures such as joints and some faults generally indicate late stage brittle responses that cannot be easily

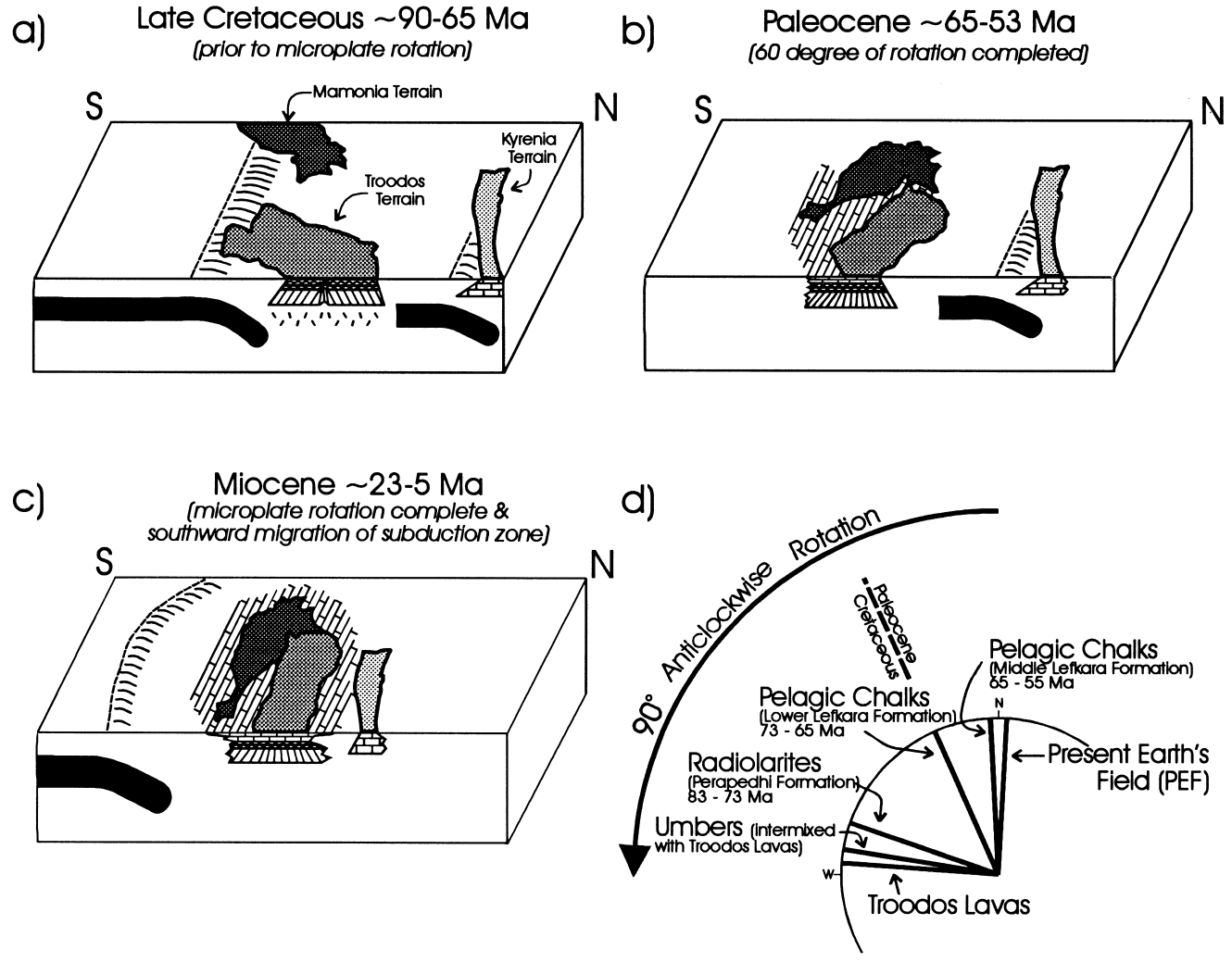

Fig. 3. (a–c) Block diagrams showing the tectonic evolution of Cyprus. N and S refer to the present North and South with the map view of the tectonic elements in their present orientation (mainly from the work of Robertson, 1990). (d) The rotations of the cover rocks and the underlying tectonic units as revealed by paleomagnetic studies (Clube and Robertson, 1986).

related to long-term regional deformation patterns, although they have been investigated in Cyprus (Lapierre et al., 1988; Orsag-Sperber et al., 1989; Grand et al., 1993; Payne and Robertson, 1995). For this reason, we supplemented the observations on stylolitic cleavage, the only field microstructure that reveals penetrative strain (Fig. 5), with rock-magnetic techniques that define cryptic alignments of minerals.

3. Magnetic fabrics

Mineral alignments, defining a planar–linear fabric (schistosity–lineation, or S–L) could be described by ellipsoids reflecting the orientation distribution of crystallographic axes. The same arguments can be applied to grain shapes giving rise to the L–S fabric scheme of Flinn (1965). It is important to remember that such fabric types run a smooth spectrum from oblate (S) through flat-shaped ($S > L$), neutral ($S = L$), constricted ($S < L$) to prolate (L). Since a single, penetrative orientation–distribution of crystal or grain shapes is congruent with an ellipsoidal shape it may have only axial or orthorhombic symmetry (Flinn, 1965). Contrasting views arise from the common misapplication of the description of Turner and Weiss (1963), of combined, competing subfabrics, and one may still read reports of 'monoclinic' or 'triclinic' fabrics. Moreover, since magnetic fabrics are described by a magnitude ellipsoid representing the second-order tensor of low field susceptibility, they are invariably orthorhombic or axial (Owens, personal communication, 1999).

In many rocks the preferred orientations of minerals may be subtle, due to fine grain size or inherently low

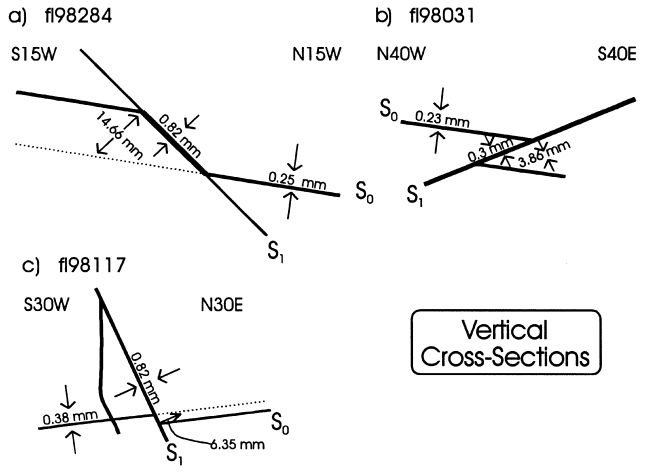

Fig. 4. Sketches show the offset of 'primary' bedding stylolites by tectonic S_1 stylolites. Tectonic stylolites are at least 50% thicker, indicating that tectonic pressure solution was much more effective in removing limestone matrix than the diagenetic processes that produced bedding-stylolites.

shape-anisotropy of the grains. In the limestones that we have studied, the small grain size would preclude much progress being made by traditional Universal stage studies with the petrographic microscope to determine the orientation–distribution of calcite (e.g. Knopf and Ingerson, 1938).

Magnetic methods are now known to be successful in revealing the fabrics of many types of rocks: sedimentary rocks, igneous rocks, metamorphic rocks and weakly strained sedimentary rocks (Tarling and Hrouda, 1993; Borradaile and Henry, 1997). The power of the magnetic method is that it can determine the preferred orientation of all grains in a sample in a few minutes. The typical cylindrical sample has a volume of 11.5 cm^3 so that in the case of our fine-grained, pelagic limestones, the mean orientation is determined for thousands of grains.

The most common method measures the anisotropy of the sample's susceptibility to induced magnetism. The power of this method is its speed; about 3 min per sample. Common rock-forming silicates normally have mean susceptibilities < 2000 μSI and commercially available equipment such as the Sapphire Instruments system or the AGICO Kappabridge easily produce a precision of < 1 μSI so that the sensitivity is high. In terms of fabric directions, the 95% confidence limits about the principal directions are commonly $< 5°$ for routine work on tectonic fabrics such as those in slates. Referred to as AMS, *anisotropy of magnetic susceptibility*, the procedure involves the application of a weak field (~0.1 mT) to avoid any significant permanent magnetization of remanence-bearing phases such as magnetite. We apply the field in seven different directions that include body-diagonal (⟨111⟩) directions. This choice of directions provides seven measurements from which the tensor of low field susceptibility anisotropy is determined (Borradaile and Stupavsky, 1995).

The interpretation of AMS involves the assessment of the relative contributions of three types of magnetic behaviour and each mineral may respond in one of those three ways, according to its composition. To appreciate this, we must start by considering the mean or bulk susceptibility, setting aside anisotropy for simplicity. The first type of physical response, diamagnetism, is universal. This yields a weak negative susceptibility (~ -14 μSI) and it is the only response from minerals such as calcite, quartz and feldspar, although inclusions may easily mask the diamagnetism. The second is the paramagnetic response, shown by the majority of rock-forming silicates, such as clays, micas, and mafic silicates in general. This is parallel to the applied field and is thus positive. Its value varies with the mineral structure and composition but for most rock-forming minerals it does not normally exceed +2000 μSI. For clay minerals in our limestones the

paramagnetic response is a few hundred μSI. The third response comes from minerals that can carry permanent magnetization, loosely referred to as *ferro*magnetic. In our limestones, magnetite traces, probably derived from the magnetosomes of fossil magnetotactic bacteria (e.g. Butler, 1992) are the significant remanence carriers, although goethite and hematite may be present as minor weathering products. The susceptibility of magnetite is very high, from 2×10^6 to 5×10^6 μSI, so that negligible traces offset the contributions from a diamagnetic calcite matrix, or a paramagnetic clay mineral fabric even though those minerals are much more abundant. Therefore, interpretation of AMS must take into account relative abundances, mean susceptibilities and anisotropies of minerals. The magnitudes of AMS sometimes reflect more the rock composition than intrinsic fabric intensity (Borradaile, 1987). The differences in the mineral anisotropies may be considerable; sheet silicates have high anisotropies, whereas those of calcite and quartz are low (Hrouda, 1986; Borradaile and Werner, 1994; Borradaile and Henry, 1997; Hrouda et al., in review). The weak anisotropy of magnetite is controlled by grain shape rather than crystallographically due to its high susceptibility and the effects of its demagnetizing field.

The principal AMS directions cannot always be interpreted literally as the principal directions of any particular mineral fabric (e.g. Woodcock, 1977), because the whole-rock AMS is the result of multiple minerals, each with different magnetic responses, different anisotropies and perhaps with different orien-

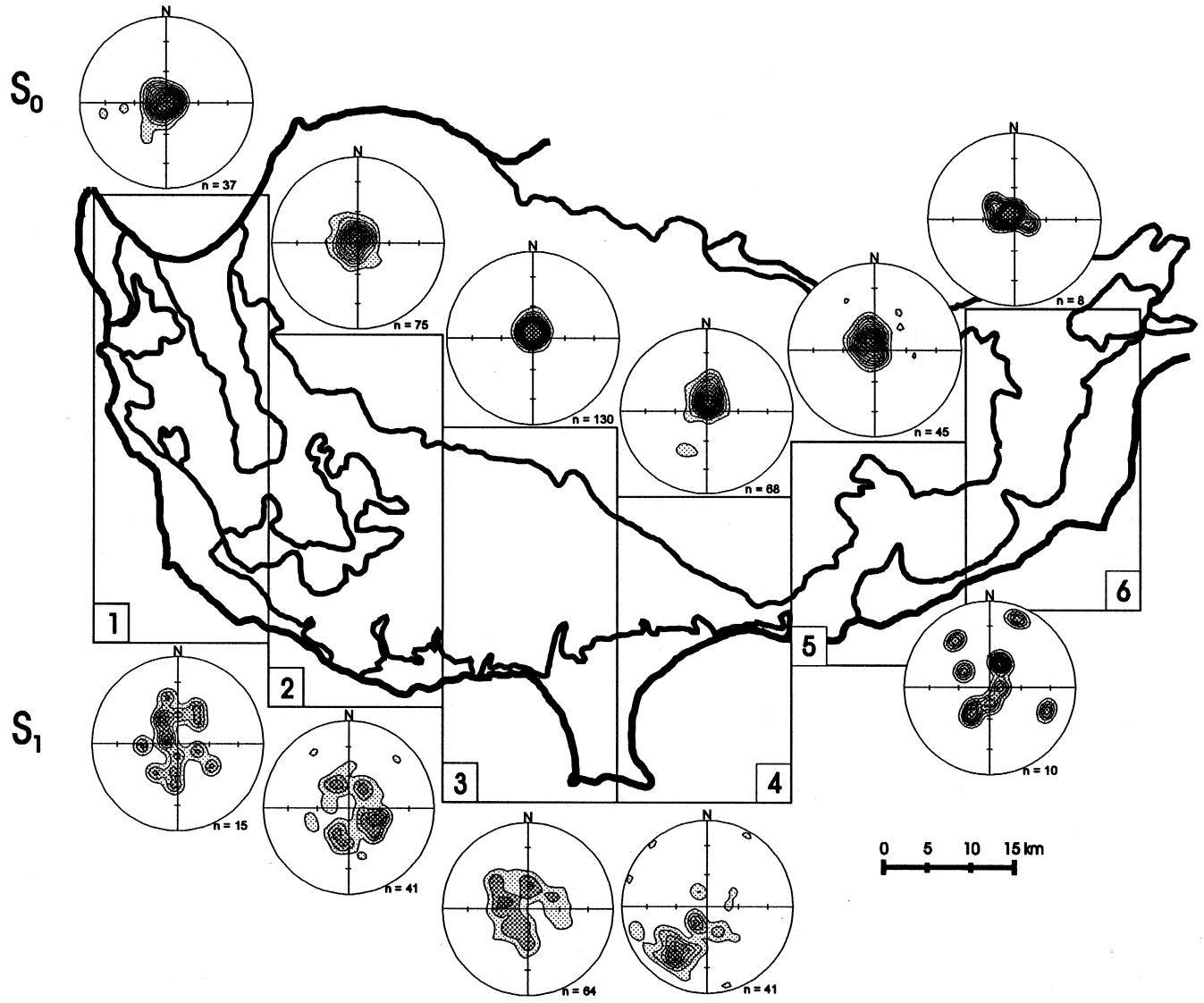

Fig. 5. Orientations of bedding (S_0) and stylolitic cleavage (S_1) grouped in six domains in the sedimentary cover of southern Cyprus. (Lower hemisphere, equal area stereonets.)

tation distributions (Borradaile and Henry, 1997). These complications are all the more relevant where, as in this study, some minerals have a sedimentary fabric and others a tectonic one: their orientation distributions blend their individual AMS contributions into those of the sample's AMS. Moreover, even for a monomineralic rock the principal directions of the anisotropy ellipsoid only represent the Eigen directions of the mineral orientation distribution; they cannot be interpreted literally as finite strain directions, although there may be some correlation (Borradaile, 1991). The noncoaxiality of most finite strain histories (e.g. Ramsay, 1967; Ramsay and Huber, 1983) may give rise to the same problem. In some rocks, the principal directions may correspond to *stress* orientations at the time of crystal nucleation and have little to do with finite strain (Borradaile and Henry, 1997).

Using the fact that some accessory minerals, mostly iron oxides and some iron sulphides bear a remanence, a new dimension has been added to the study of magnetic fabrics in recent years (Jackson, 1991; Jackson and Tauxe, 1991; Rochette et al., 1992). This measures the anisotropy of successively artificially applied remanences, in different directions. Early studies used direct field remanences (isothermal remanence magnetization, IRM) and although this is usually successful it risks a nonlinear susceptibility response if the field has to be increased greater than, say 10 mT, to achieve measurable remanences (Daly and Zinsser, 1973; Borradaile and Dehls, 1993). Consequently a more elaborate technique, *anisotropy of anhysteretic remanence* (AARM) was developed to use a small applied field ~0.1 mT (McCabe et al., 1985). To permit this small field to produce a significant remanence it is applied while the sample is exposed to a steadily decaying alternating field. The DC field thus biases the scattering of spin moments during alternating field demagnetization. We applied ARM in seven directions and from the remanences produced in each direction the ARM tensor was determined and thus the AARM ellipsoid, comparable to the AMS ellipsoid. The details of our technique, including a discussion of the problems of interstep demagnetization may be found in Werner and Borradaile (1996). In this study, the DC bias field was applied during the decay of the AF from a peak value of 60 mT to 0 mT: pilot studies showed that this sufficed to saturate the magnetite component in the limestones.

In this study, although all samples bear evidence of magnetite content, only 201 of the 1170 limestone samples carried enough magnetite to yield a well-defined AARM that permitted comparison with AMS. For the purposes of interpretation, our rocks are in this instance quite simple. AMS combines the preferred crystallographic orientation fabric of clays with a preferred dimensional orientation fabric for magnetite grain shapes. On the other hand, AARM isolates the preferred dimensional orientation of magnetite. Elsewhere, an algebraic technique has been attempted to subtract the AARM tensor from the AMS tensor (Borradaile et al., 1999) but it requires a sensitive normalization procedure and the absence of any superparamagnetic contribution (Hrouda et al., in review); it was unsuccessful in this study.

4. Magnetic mineralogy

Our investigation of magnetic mineralogy has chiefly used susceptibility measurements (Sapphire Instruments induction coil) and hysteresis measurements (Princeton Measurements Micromag). The latter provide hysteresis loops that, when corrected for the susceptibility of the diamagnetic or paramagnetic matrix, compare with published values for pseudosingle domain (PSD) magnetite (Table 1). From the hysteresis parameters H_c (coercivity), H_{cr} (coercivity of remanence) and the ratio of zero field remanence to saturation remanence (M_r/M_s) we are able to recognize this behaviour for 170 samples. These data are normally presented on two types of plots (Wasilewski, 1973; Day et al., 1977). However, we find it convenient to combine these into a single three-dimensional plot (Fig. 6). This shows us that single-domain magnetite is absent: this is fortunate because it produces inverse fabrics (k_{MAX} parallel to the short grain axis, etc.) that could complicate petrofabric interpretation (Rochette et al., 1992). It is evident according to all criteria that the magnetite shows a large pseudosingle domain response and therefore we can expect the AMS contribution of magnetite to reflect faithfully its orientation distribution. In fact, inverse fabrics, or composite inverse–normal fabrics due to single-domain magnetite are very rare, and the extreme possibility that some small PSD grains could cause inverse fabrics is still less probable.

A further value of the three-dimensional hysteresis plot is the clarification of trends. Fig. 6(e) shows that the regression surface becomes progressively shallower (M_r/M_s lower with respect to both H_c and H_{cr}) as the depth of deposition becomes shallower. This may be due to changing proportions of bacterial vs. clastic magnetite as the depositional environment changes (Butler, 1992; Borradaile et al., 1993b).

We determined the susceptibility of the matrix that supports the magnetite inclusions from the slope correction of the hysteresis loops (e.g. Richter and van der Pluijm, 1993; Borradaile and Werner, 1994). Although the chalks and limestones are invariably white, their clay content is sufficient that 88% of the samples show a paramagnetic matrix susceptibility due to the paramagnetism of the clays, dominating over

Table 1
Hysteresis parameters compared with values for single domain (SD) and multidomain (MD) magnetite (Dunlop and Özdemir, 1997)

Parameter	Dunlop SD	Dunlop MD	Mean	Standard deviation	Standard error
H_c (mT)	10–40	2.5–4	14.50	13.23	1.02
M_r/M_s	0.5–0.9	0.01–0.03	0.18	0.056	0.004
H_{cr}/H_c	< 2	> 4	2.162	0.496	0.04

the diamagnetism of the calcite matrix. The remaining 12% of samples have negative susceptibilities, where diamagnetic calcite dominates the susceptibility response.

Bulk susceptibility measurements using the AMS induction coil for the 1170 samples used in AMS determination have a mean value of 45.3 ± 6.1 μSI. Of the samples, 83% range between -15 μSI and $+60$ μSI with no sample > 500 μSI (Fig. 7a). However, calculation shows that these bulk susceptibilities can arise with combinations of $\ll 0.01\%$ magnetite and $> 0.1\%$ clay content (Table 2). Normally, the fabric of the diamagnetic calcite matrix is overwhelmed by the fabrics of the accessory clays and magnetite, not just because of their higher bulk susceptibilities but also because of their strong preferred orientations and the high anisotropy of the phyllosilicate. The hysteresis measurements show that the *bulk* susceptibility due to remanence bearing phases (K_{ferro}) forms more than half of the total susceptibility in 71% of samples (Fig. 7b). However, this does not mean that the *anisotropy* of magnetite is dominant, as explained below.

5. Interpretation of magnetic fabric orientations

AMS fabrics, combining the contributions from clay minerals and magnetite, in most cases have been obtained from 1170 samples drilled from 434 oriented blocks sampled at 385 outcrops (Fig. 1b). The poles to AMS foliations cluster tightly, indicating dips of $\sim 10^\circ$ and the AMS lineations are N–S directed with some slight radial divergence southwards from the Troodos Complex (Fig. 8). The AMS foliations are locally inclined to bedding and the well-defined AMS (k_{MAX}) lineation transects tectonic structures so that the AMS is strongly influenced by regional tectonics. Thus, we cannot accept a purely sedimentary origin for these AMS fabrics. The AMS fabrics represent a predominantly tectonic, L–S fabric of clays and magnetite, broadly indicating N–S extension or mineral alignment with gently dipping AMS foliation planes distinct from bedding, especially at the site level and thus clearly tectonic. However, they are not parallel to S_1, identified in the field, indicating age differences between S_1 and AMS. The foliation poles form clusters but these disperse into minor girdles in the EW direction. Thus the AMS lineation, which is perpendicular to this, may be interpreted as the zone-axis to the clay-mineral fabric. Of course, this combines with the grain-shape lineation of magnetite grains to yield the overall AMS fabric. The consistently oriented AMS fabric indicates N–S stretching of the limestone sequences.

AARM fabrics isolate the contribution of magnetite's preferred dimensional orientation. AARM foliations vary more between subareas than the S_1 and AMS fabrics. However, they transect primary structures locally so that they are at least partly tectonic in origin. Moreover, magnetite fabrics normally postdate AMS fabrics so that we do not doubt a strong tectonic influence on AMS. It dips $\sim 45^\circ$ in area 1, and slightly shallower to the NW in areas 2 and 3. Gentler dips occur in the eastern subareas 5 and 6 (Fig. 9). The AARM lineation defining the alignment of magnetite grains is dominantly NE–SW, with two less significant directions found in the localized Yeresa fold and thrust belt (Fig. 2). Inspection of the orientations of bedding, cleavage and AARM foliation, particularly at the site level, commonly reveal that the AARM lineation may be a composite sedimentary–tectonic magnetic intersection–lineation due to the interference of AARM foliation and bedding fabrics

Table 2
Theoretical range of bulk susceptibility calculated using simplified values, but approximating those of published data (Carmichael, 1982; Dunlop and Özdemir, 1997, p. 23) of constituent minerals

Accessory mineral	Accessory mineral with $k > 0$ 0.1% of volume	Diamagnetic calcite matrix 99.9% @ average $k \approx -10$ μSI	Sample k = Accessory + Matrix
Magnetite 5 000 000 μSI	5000 μSI	−9.99 μSI	4990.01 μSI
Clay 1000 μSI	1 μSI	−9.99 μSI	−8.99 μSI

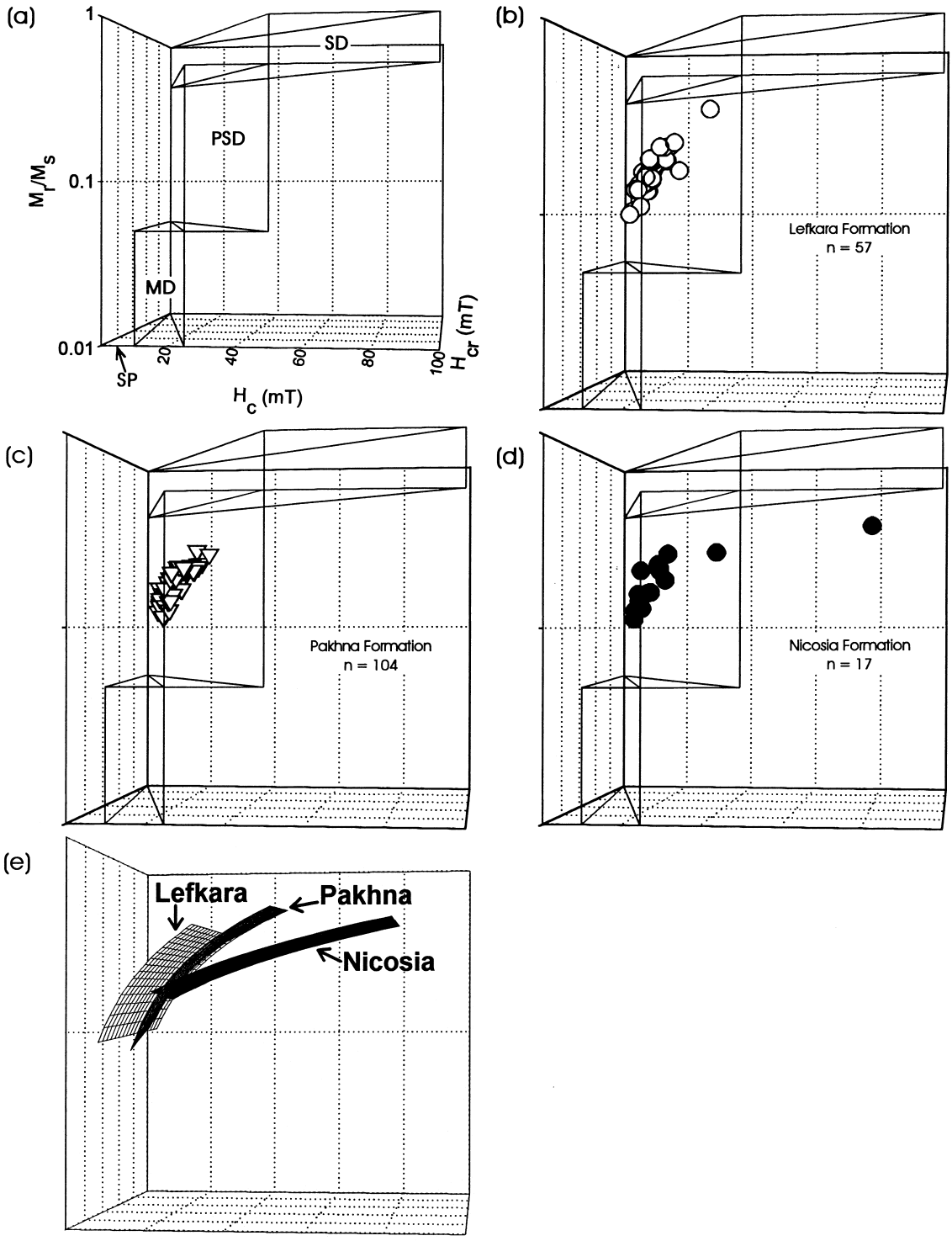

Fig. 6. (a) A new projection classifying the magnetic response of magnetite according to superparamagnetic (SP) single-domain (SD), pseudo-single domain (PSD) and multi-domain (MD) behaviour. This uses the hysteresis parameters coercivity (H_c), coercivity of remanence (H_{cr}) and the ratio of zero field remanence (M_r) to saturation remanence (M_s). Normally the characterization of magnetic behaviour requires two graphs (H_c vs. H_{cr}, Wasilewski, 1973; M_r/M_s vs. H_c/H_{cr}, Day et al., 1977) but their combination in three-dimensions facilitates discrimination of the behaviour. (b) Our data from the Lefkara Formation include 57 pelagic limestone samples. (c) The Pakhna Formation is represented by 104 pelagic to shallow water limestones. (d) The Nicosia Formation is represented by 17 shallow water limestones. All 178 limestone samples show PSD behaviour close to the SD field. (e) Best-fit planes show that a progressive change in magnetic parameters of accessory magnetite occurs with the depth of sedimentation, perhaps due to changing sources of magnetite (e.g. bacterial vs. clastic).

(Fig. 10), (Borradaile and Tarling, 1981; Housen and van der Pluijm, 1991; Housen et al., 1993a). Thus, AARM lineations are not parallel but rather perpendicular to tectonic extension. Therefore, we may infer that the tectonic extensions are WNW–ESE.

6. Comparison of field and magnetic fabrics

6.1. Fabric orientations

The paucity of folds, the localization of cleavage

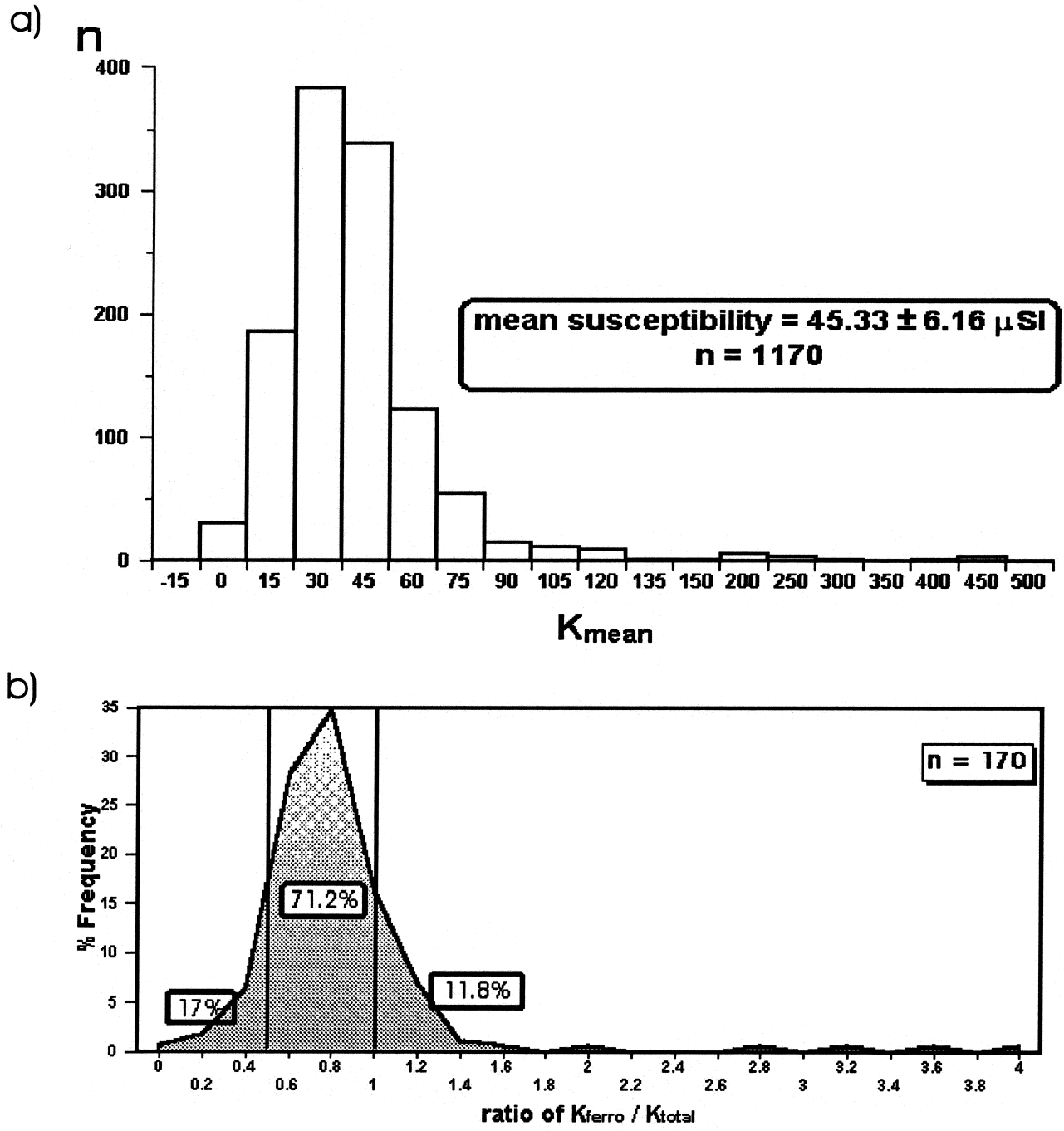

Fig. 7. (a) Bulk susceptibilities used in the AMS study. (b) Frequency distribution of the ratio of ferromagnetic susceptibility (K_{ferro}) to bulk susceptibility (K_{total}). These values were derived from slope corrected hysteresis loops of 170 selected samples (mean sample size $\approx$0.004 g). $K_{total} = K_{ferromagnetic} + K_{paramagnetic} + K_{diamagnetic}$. The ratio may exceed unity where the matrix is diamagnetic (negative susceptibility). In 71% of samples the ferromagnetic contribution of magnetite provides more than 50% of the *bulk* susceptibility. However, the low anisotropy of magnetite permits clay minerals with lower bulk susceptibilities but higher anisotropies to dominate AMS. In only 17% of samples does paramagnetic clay dominate over the bulk susceptibility contribution of magnetite traces.

development and absence of grain-alignments visible in the field leaves few traditional field techniques to permit an evaluation of the structural history. Thus, we have used S_1–S_0 angular relationships, in particular vergence, to infer the kinematic pattern associated with S_1 cleavage formation. Generally, bedding is subhorizontal or shows only low, southerly dips, $< 10^\circ$ (Fig. 5). S_1 inclinations are generally, and at the level of individual sites, northerly-dipping. Thus, *in general*, the S_1 planes lean or verge to the south with respect to bedding. This indicates southerly-directed 'overthrust' motion, i.e. the overlying strata have been sheared or moved southward relative to those underlying them. Only zone 4 shows a consistent vergence direction, to the SSW, due to localized Early to Middle Miocene uplift causing the more severe tectonism of the Yeresa fold and thrust belt on the coast in subarea 4. This small area (approximately $25 \times 3\,km^2$) is also anomalous in its AMS and AARM fabric orientations that are of local rather than regional significance and are not included in this regional study.

More specifically, at the site and local level, S_1–S_0 vergences reveal systematic differences between subareas (Fig. 11a). This shows that, in detail, the vergences cannot be explained solely by the regional compression of Cyprus, for example, associated with the northward subduction direction over the last 50 Ma (Fig. 3). Instead, the vergence patterns reveal localized variations in the regional compression due to gravity sliding into several local sedimentary basins (Polemi, Akrotiri, Pissouri) and away from the SW, S and SE slopes of the Troodos terrain (Fig. 12). The pressure solution cleavage appears to be the earliest tectonic fabric because the shallower AMS foliation cuts across it.

AMS foliation is more consistently oriented than S_1

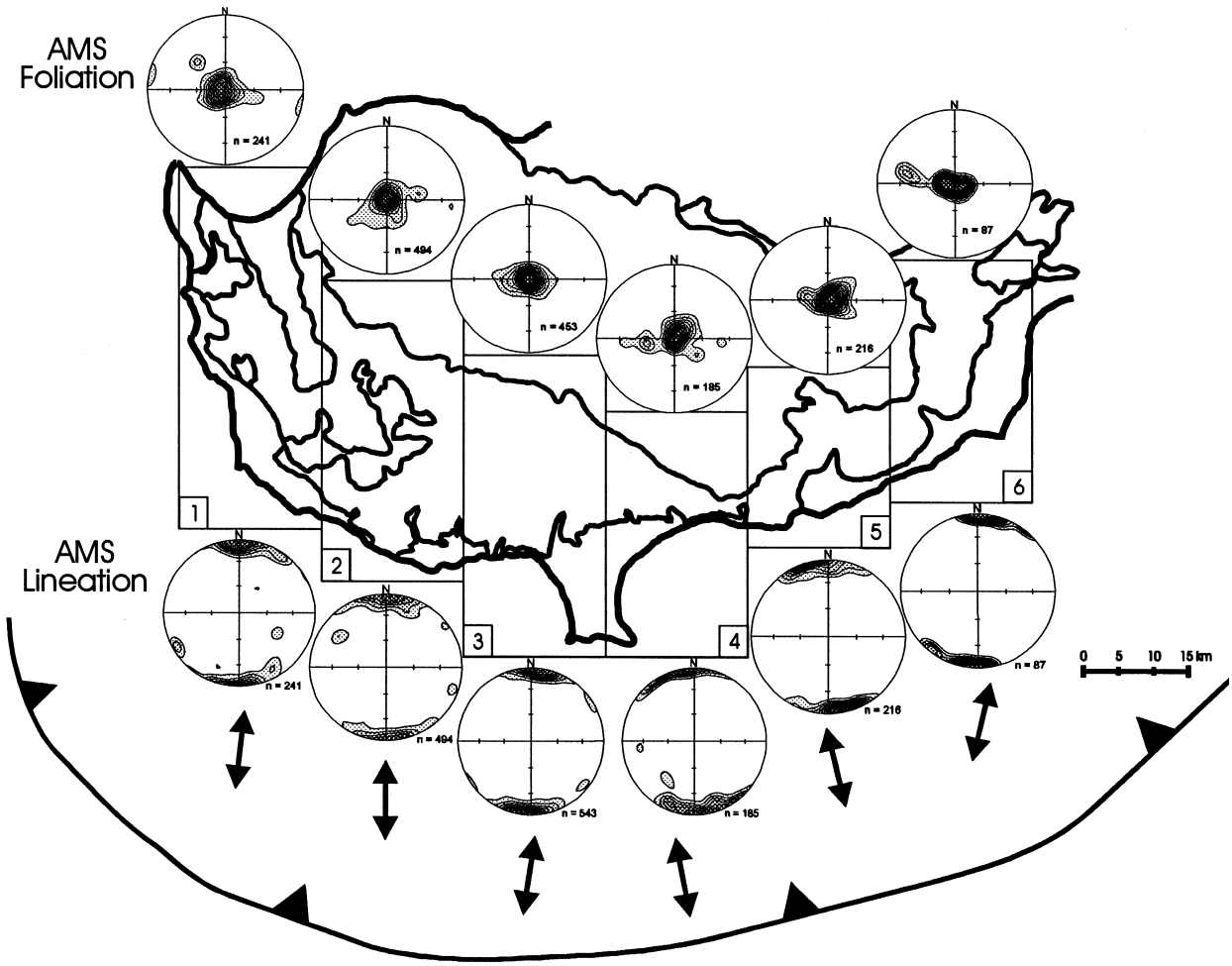

Fig. 8. Fabrics shown by anisotropy of magnetic susceptibility (AMS) in six domains of the sedimentary cover of southern Cyprus. Upper stereonets show the distributions of minimum susceptibility, which correspond to the poles of the magnetic foliation. This, in turn, represents the orientation distribution of basal planes to clay minerals. Although magnetite traces contribute more to the bulk susceptibility, the low anisotropy of that mineral does not greatly influence the AMS fabric. The lower stereonets show the maximum axes of susceptibility, corresponding to long axis alignment of clay crystals. (Lower hemisphere, equal area stereonets.) The arrows indicate the average inferred extension directions.

in each subarea and, as with S_1, we may consider its vergence with respect to bedding (AMS–S_0). Normally when using vergence in structural geology, a tectonic planar fabric S_n should be referred to the orientation of the previous planar structure S_{n-1}. However, in this study, the first planar structure, bedding, is so feebly disturbed that it may be used as the reference surface for the definition of vergences for S_1, as well as for the vergences of AMS-foliation and AARM-foliation. Whereas S_1–S_0 vergences relate to the pre- and early Miocene uplift of Troodos, and basin depression (Figs. 11 and 12), the subsequently developed, cross-cutting AMS fabric is regionally controlled (Figs. 8 and 11). AMS–S_0 vergence is therefore also controlled at the regional level, showing a southward, barely radial movement pattern away from the Troodos range (Fig. 11b). This corresponds to a later phase in the uplift history, when basin subsidence was insignificant and Troodos uplift dominated the picture, with AMS lineations indicating stretching radially away from the Troodos terrain as the stratigraphic sequence was extended by gravity sliding.

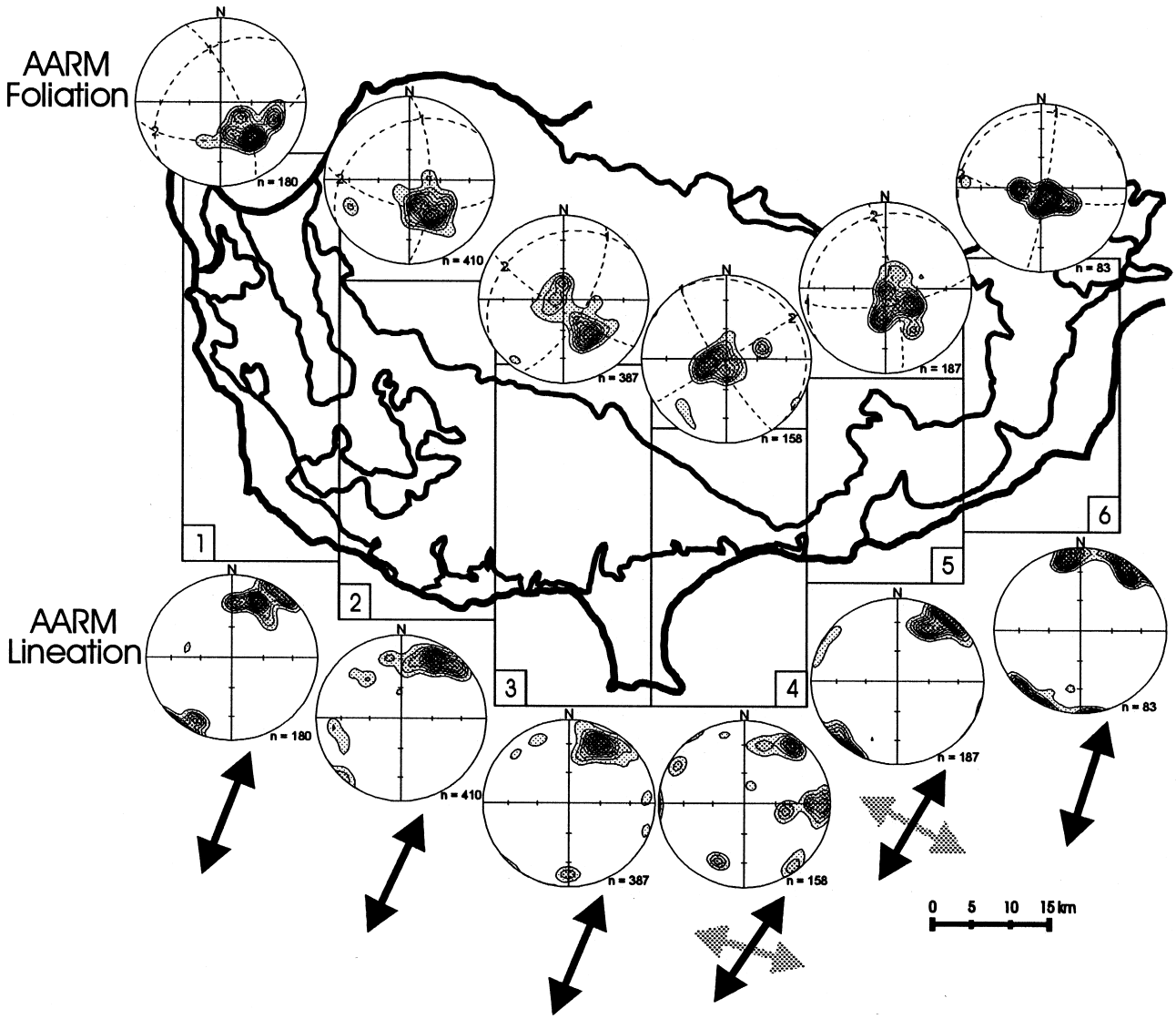

Fig. 9. Fabrics shown by anisotropy of anhysteretic remanence (AARM) in six domains of the sedimentary cover of southern Cyprus. Upper stereonets show the distributions of minimum axes, which correspond to the poles of the AARM foliation. This represents the *S*-plane of the shape-orientation fabric of the magnetite grains. The principal fabric planes are shown intersecting at the minimum (1), intermediate (2) and maximum (3) principal (Eigen) directions. The lower stereonets show the maximum axes, corresponding to long axis alignment of magnetite. (Lower hemisphere, equal area stereonets.) The principal alignment is shown by bold arrows, but in two subareas, some outcrops show a nearly orthogonal lineation, indicated here as greyed arrows. However, these alignments are not believed to indicate the true extension directions but may result from an incomplete tectonic overprint of the sedimentary AARM fabric (Fig. 10). The actual movement directions for the AARM fabric are more reliably given by AARM–S_0 vergence (Fig. 11c).

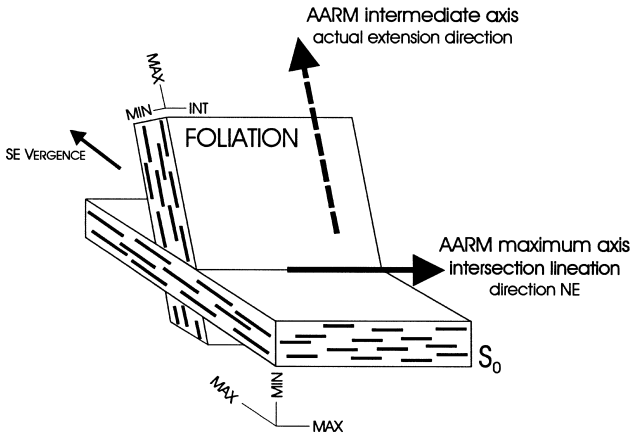

Fig. 10. AARM fabrics have maximum axes (lineation) parallel to the intersection of bedding (S_0) and stylolitic cleavage (S_1). This is due to the combination of planar tectonic foliation and an incompletely overprinted bedding fabric so that their intermediate axes combine to produce a net maximum parallel to S_0–S_1 intersection lineation (e.g. Borradaile and Tarling, 1981).

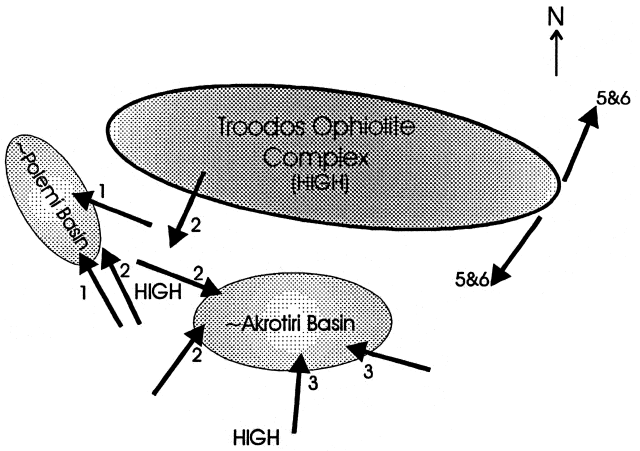

Fig. 12. Sketch showing the movement directions inferred from S_1 vergences outlined in Fig. 11(a). Radially gravity sliding from Troodos dominates, with subordinate gravity sliding into localized sedimentary basins. The number associated with each arrow identifies the corresponding subarea. S_1 vergence directions of subarea 4 are omitted since they are not the result of gravity sliding (see text for explanation).

AARM fabrics developed still later, cross-cutting earlier fabrics. Interpretation of their principal directions is not immediate, because the AARM fabric combines contributions from a bedding fabric of magnetite and a tectonic–stylolite fabric inclined to bedding (Fig. 10). Clearly the AARM foliations verge ESE. Thus, the magnetic lineation (Fig. 9) is perpendicular to the extension direction causing the tectonic alignment of magnetite. This extension direction is WNW–ESE, unrelated to Troodos uplift. The SSE vergence of AARM–S_0 (Fig. 11c) is the most consistent of the three fabric types.

The contribution of magnetite to the AMS fabric orientations may be achieved by comparing Figs. 8 and 9, especially the lineations. Particularly in zones 1, 2, 5 and 6, we see that AMS maxima skew towards the AARM maxima directions. This shows that although the magnetite contributes most of the *bulk* susceptibility, its *anisotropy* is so low that the contribution from more anisotropic phyllosilicate dominates AMS. It is commonly reported elsewhere that pseudo-single domain and multi-domain magnetite grains have a low shape-anisotropy and thus a low magnetic anisotropy. In our limestones and chalks the magnetite is largely of bacterial origin, in the form of equidimensional magnetosomes (Butler, 1992) that are expected to have very low magnetic anisotropy.

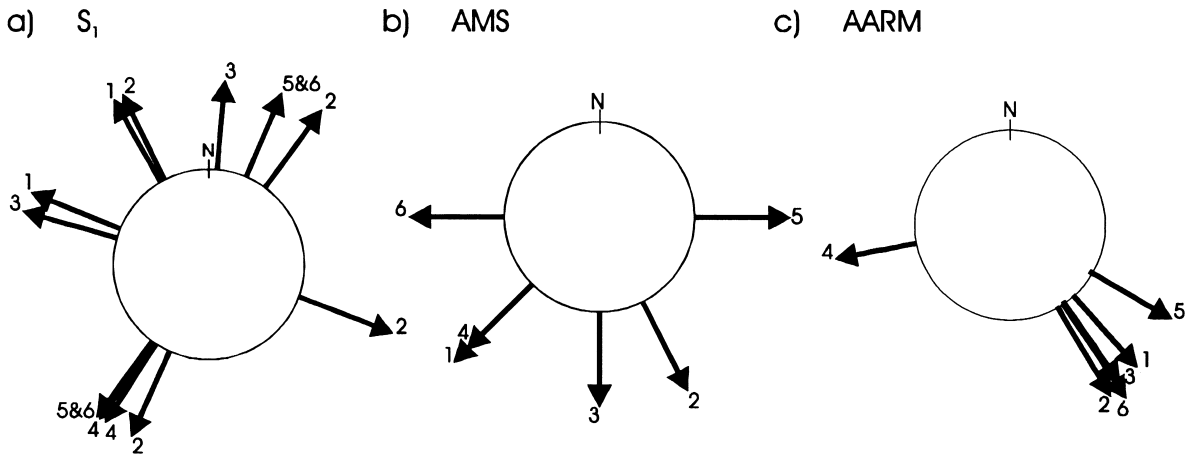

Fig. 11. The vergence directions of the tectonic planar fabrics with respect to bedding. These indicate the direction of over shearing of the nearly horizontal stratigraphic sequence during the progressive development of (a) stylolitic cleavage, (b) phyllosilicate alignment (AMS) and, finally, (c) alignment of magnetite (AARM).

6.2. Fabric shapes

The shape of the fabric ellipsoid is best represented by an intensity parameter P_j (equal to 1 for a sphere) and a shape parameter T_j ($+1$ = oblate; 0 = neutral; -1 = prolate). These parameters, introduced by Jelinek (1981) are defined in the Appendix. In structural geology, the Flinn (1965) diagram is usually used to plot fabric or strain ellipsoids, with the ratios a (max/int) and b (int/min). The Flinn plot has the advantage of providing an easily visualized, familiar representation. However, fabric shape, the degree of prolateness or oblateness is not represented by an axis but by the slope of a line from the origin to a data point, and that slope is a nonlinear representation of shape (flat ellipsoids have slopes 0–1; rod-shaped ellipsoids may have slopes between 1 and ∞). Furthermore, neither is the eccentricity of the ellipsoid (intensity of strain, or fabric development) fixed to an axis. On the contrary, the Jelinek parameters provide a linear representation of fabric shape on the vertical axis and a logarithmic representation of eccentricity on the horizontal axis.

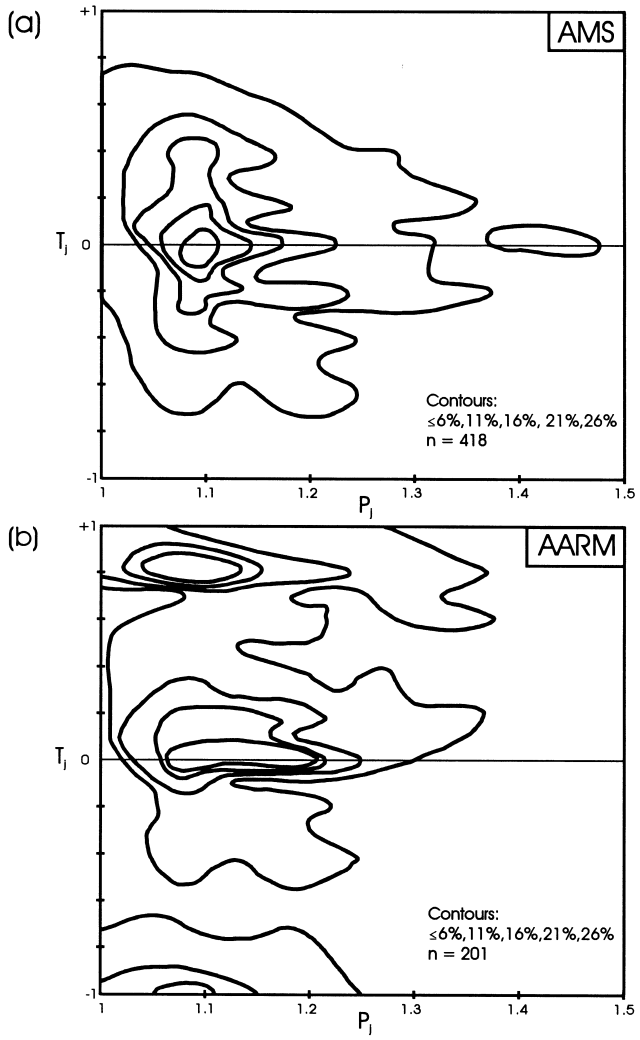

Fig. 13. Fabric plot of P_j and T_j parameters (Jelinek, 1981); $T_j = 1$ for oblate, $T_j = -1$ for prolate. (a) AMS fabric shapes due to the preferred crystallographic orientation of clay minerals. AMS is broadly distributed about $T_j \approx 0$, reflecting the combination of more oblate crystallographic symmetry of clay minerals with the more prolate symmetry of the magnetite AARM fabric. (b) AARM fabric shapes due to the preferred dimensional orientations of pseudo-single domain magnetite. Note that the magnetite fabric shapes are bimodal, probably due to the combination of bedding fabrics ($T_j \approx 1$) and tectonic fabrics ($T_j \approx 0$).

In general, even choosing the most convenient representation of fabric shapes, which is certainly the Jelinek Plot for magnetic fabrics, there is a tendency to over-interpret the information. First, the AMS magnetic fabric invariably blends contributions of more than one mineral, in our case, preferred crystallographic orientation of clay minerals and preferred dimensional orientation of magnetite. In this study, there may be two subfabrics of magnetite, complicating matters further at some sites. Second, the complexity of interpretation is compounded because in some instances a sedimentary fabric is combined with a tectonic one, making fabric shapes difficult to interpret. Even if the fabric was solely tectonic, the aligning mechanism is unknown and unquantifiable so that it is inappropriate to speculate about relative stress magnitudes during nucleation or finite strain during alignment.

Thus, in this study, we may only compare AMS with AARM fabric shapes in the most general sense. For example, AARM fabric shapes dominate the field of flat shaped ellipsoids ($1 > T_j > 0$) with two distinct modes, one neutral-shaped ($T_j \sim 0$) and one almost perfectly oblate ($T_j \sim +1$) (Fig. 13). The former is readily interpreted as the combination of equally developed planar ($T_j \sim +1$) tectonic and bedding fabrics of magnetite (Fig. 10). The latter may represent a planar bedding fabric where stylolitic cleavage is weakly developed.

The AMS fabric shapes are unimodally distributed, clearly concentrated at the neutral shape position ($T_j \sim 0$) and skewed toward the oblate ($T_j > 0$) field (Fig. 13). This is compatible with a more homogeneous, single-event fabric with a broad range of L–S fabric types. Interestingly, the AMS and AARM fabrics show an equal range of P_j values, representing the eccentricity or intensity of the fabric ellipsoid. Elsewhere, it is commonly found that AARM intensities exceed those of AMS from the same rocks. However, the similarity here is due to the fact that a portion of the AMS fabric is due to magnetite that has a broad, bimodal range of fabric types, as revealed by AARM, and that AMS is controlled by phyllosilicates that have some of the highest anisotropies amongst silicates.

7. Conclusions

The combination of observations of field structures and magnetic petrofabrics reveals the kinematic pattern of the southern half of Cyprus, mainly associated with the uplift of Troodos, during its ductile periods of deformation, before the faulting and jointing. The first microstructural event recorded in the sedimentary cover is the development of a stylolitic S_1 cleavage that is 50% more effective than primary bedding stylolites in removing calcareous matrix. Nevertheless, S_1 is only locally developed and also commonly weakly developed. Its vergence with respect to the barely disturbed bedding shows that the sedimentary sequence slipped gravitationally. The movements were radially away from the domal uplift of Troodos, and radially inwards to localized sedimentary basins.

Subsequently, mild penetrative deformation aligned clay minerals in the bulk of the limestone and chalk mainly by pressure solution. This fabric is mainly revealed through AMS, although trace magnetite also contributes a little to the AMS signal. The vergence of the AMS foliation shows that the south-directed movement away from the Troodos range continues, but is now constant in orientation across the area, unaffected by the location of sedimentary basins. The AMS lineation represents the zone axis of phyllosilicate alignment (L–S fabrics) showing that stretching of the sedimentary cover was consistently N–S, transecting local tectonic perturbations of bedding. The AMS fabrics are clearly tectonically dominated and the degree of regional consistency in orientations is compatible with a supra-subduction setting of the sedimentary sequence (Robertson, 1990).

We established the magnetite petrofabric via AARM. This has a consistent, and unusual foliation vergence, to the ESE, transecting local perturbations of strata. The ESE directed push cannot be reconciled with the uplift of the Troodos ophiolites. However, Cyprus lies on the southern margin of the Anatolian block that has been rotating anticlockwise against the Cyprian Arc subduction zone (Rotstein, 1984). Thus, we may explain the ESE vergent AARM foliation as a consequence of dextral transpression on the north side of the Cyprian Arc as the Erastothenes Seamount is being subducted northward from the WSW of Cyprus (Xenophontos, personal communication, 1999).

In terms of rock magnetic techniques we found it most useful to devise a three-dimensional plot of hysteresis parameters to confirm the pseudosingle domain response of the magnetite. This was necessary to discount any inverse-fabric complications of single domain magnetite. Another innovation was the use of vergence of magnetic foliation. This permits *one* magnetic fabric to provide a shear sense, whereas previously a combination of two was normally used (Borradaile and Spark, 1991; Borradaile and Dehls, 1993; Borradaile et al., 1993a). In the case of AARM, the perpendicular directions of vergence and AARM lineation (confirmed by outcrop relations of structures) confirm that the magnetic fabric is composite. Composite bedding-tectonic fabrics producing a magnetic lineation parallel to foliation–bedding intersection have been reported before, in isolated examples (e.g. Borradaile and Tarling, 1981) but not as extensively and uniformly on a regional scale.

Principal directions of tectonic magnetic fabrics are readily interpretable in most instances, as long as one is aware of the possibilities of incompletely overprinted primary fabrics and of metamorphic recrystallization (Borradaile and Henry, 1997). On the other hand, the interpretation of fabric shapes (T_j parameter) is much more complex as it reflects the combination of different magnetic responses (paramagnetic, diamagnetic and 'ferromagnetic'), from several minerals that may have different orientation distributions. Thus, despite an initial optimism in the scientific literature, rarely do the shapes of susceptibility magnitude ellipsoids (e.g. represented by T_j) or eccentricities/intensities (e.g. represented by P_j) correlate with the shape of a strain or stress ellipsoid or of any other causative alignment process such as primary flow mechanisms (Borradaile, 1991). Attempts to isolate the fabric contributions of different magnetic responses (e.g. diamagnetic vs. paramagnetic) or of different minerals by experimental (Borradaile et al., 1987; Rochette and Fillion, 1988; Borradaile and Sarvas, 1990; Richter and van der Pluijm, 1993; Borradaile and Henry, 1997) or theoretical approaches (Henry, 1983; Rochette, 1987; Housen and van der Pluijm, 1990, 1991; Housen et al., 1993a, b; Borradaile et al., 1999; Hrouda et al., in review) have not yet made sufficient progress to facilitate tectonic interpretations.

However, by combining AARM and AMS fabric shapes on a single graph, it is possible to make some limited but useful deductions. Firstly, the AMS and AARM fabric shapes show similar patterns on the Jelinek Plot for each subarea. Thus, the fabric ellipsoid shapes are controlled by similar processes throughout and we may infer that these processes are regionally, rather than locally controlled. One can observe the contribution of AARM to AMS, qualitatively, from the relative degree of saturation of the two fabrics and the contrast in shape in the L–S spectrum (i.e. $L > S$, $L = S$, etc.), see Fig. 13.

Acknowledgements

We are indebted to the Geological Survey of Cyprus, through its Director Dr. G. Constantinou and Assistant Director Dr. S. Kramvis, for permission to

work, sample and export samples from Cyprus. Particular thanks are due to its Officer, Dr. Costos Xenophontos for introductory field trips and for much advice about the geology of Cyprus. This work was financed through the Natural Sciences and Engineering Research Council of Canada (NSERC) to Graham Borradaile.

Appendix

Anisotropies for AMS are conveniently summarized using Jelinek's (1981) parameters P_j and T_j, for the magnitude ellipsoid of susceptibility with axes $k_{max} \geq k_{int} \geq k_{min}$. However, the plot has advantages for plotting strain ellipsoids ($X \geq Y \geq Z$), or ellipsoids describing fabric.

P_j defines the intensity of the fabric as a measure of eccentricity of the magnitude ellipsoid:

$$P_j = \exp \times \sqrt{2\left[\left(\ln\left(\frac{k_{max}}{k}\right)\right)^2 + \left(\ln\left(\frac{k_{int}}{k}\right)\right)^2 + \left(\ln\left(\frac{k_{min}}{k}\right)\right)^2\right]}$$

where the mean susceptibility is given by

$$k = \frac{(k_{max} + k_{int} + k_{min})}{3}.$$

The advantage of P_j is that it provides a value that may be plotted on an axis, solely describing the eccentricity of the ellipsoid (cf. the Flinn diagram, on which intensity is represented by radial distance from the Cartesian origin). Moreover, the logarithmic basis of P_j disperses data near the origin and provides an even comparison of intensity differences at differing levels of eccentricity.

T_j defines the shape of the magnitude ellipsoid (degree to which the oblate or prolate condition is achieved):

$$T_j = \frac{\ln F - \ln L}{\ln F + \ln L}$$

where magnetic lineation (L) and foliation (F) are defined as:

$$L = \frac{k_{max}}{k_{int}}; \quad F = \frac{k_{int}}{k_{min}}.$$

These correspond to the ratios of dimensions, $a =$ max/int and $b =$ int/min, used to plot fabric or strain ellipsoids on a Flinn (1965) diagram in traditional structural geology.

T_j has the advantage of symmetry (prolate $= -1$, neutral $= 0$, oblate $= +1$), whereas the shape of the ellipsoid on the traditional Flinn diagram ranges from prolate $= \infty$ through neutral $= 1$, to oblate $= 0$. Furthermore, shape is represented conveniently along the vertical axis of the P_j–T_j plot.

References

Blowe, C.D., Irwin, W.P., 1985. Equivalent radiolarian ages from ophiolitic terranes of Cyprus and Oman. Geology 13, 401–404.

Borradaile, G.J., 1987. Anisotropy of magnetic susceptibility: rock composition versus strain. Tectonophysics 138, 327–329.

Borradaile, G.J., 1991. Correlation of strain with anisotropy of magnetic susceptibility (AMS). Pure and Applied Geophysics 135, 15–29.

Borradaile, G.J., Tarling, D.H., 1981. The influence of deformation mechanisms on the magnetic fabrics of weakly deformed rock. Tectonophysics 77, 151–168.

Borradaile, G.J., Sarvas, P., 1990. Magnetic susceptibility fabrics in slates: structural, mineralogical and lithological influences. Tectonophysics 172, 215–222.

Borradaile, G.J., Spark, R.N., 1991. Deformation of the Archean Quetico–Shebandowan subprovince boundary in the Canadian Shield near Kashabowie, northern Ontario. Canadian Journal of Earth Science 28, 116–125.

Borradaile, G.J., Dehls, J.F., 1993. Regional kinematics inferred from magnetic subfabrics in Archean rocks of Northern Ontario, Canada. Journal of Structural Geology 15, 887–894.

Borradaile, G.J., Werner, T., 1994. Magnetic anisotropy of some phyllosilicates. Tectonophysics 235, 233–248.

Borradaile, G.J., Stupavsky, M., 1995. Anisotropy of magnetic susceptibility: Measurement schemes. Geophysical Research Letters 22, 1957–1960.

Borradaile, G.J., Henry, B., 1997. Tectonic applications of magnetic susceptibility and its anisotropy. Earth Science Reviews 42, 49–93.

Borradaile, G.J., Keeler, W., Alford, C., Sarvas, P., 1987. Anisotropy of magnetic susceptibility of some metamorphic minerals. Physics of the Earth and Planetary Interiors 48, 161–166.

Borradaile, G.J., Werner, T., Dehls, J.F., Spark, R.N., 1993a. Archean regional transpression and paleomagnetism in Northwestern Ontario, Canada. Tectonophysics 220, 117–125.

Borradaile, G.J., Chow, N., Werner, T., 1993b. Magnetic hysteresis of limestones: facies control? Physics of the Earth and Planetary Interiors 76, 241–252.

Borradaile, G.J., Fralick, P.W., Lagroix, F., 1999. Acquisition of anhysteretic remanence and tensor subtraction from ARM isolates true paleocurrent grain alignments. In: Tarling, D.H., Turner, P. (Eds.), Palaeomagnetism and Diagenesis in Sediments, Geological Society, London, Special Publication 151, pp. 139–145.

Butler, R.F., 1992. Paleomagnetism: Magnetic Domains to Geologic Terranes. Blackwell Scientific, Boston.

Carmichael, R.S., 1982. Magnetic properties of minerals and rocks. In: CRC Handbook of Physical Constants for Rocks. CRC Press, Boca Raton, Florida, pp. 229–287.

Clube, T.M.M., Robertson, A.H.F., 1986. The paleorotation of the Troodos microplate, Cyprus, in the Late Mesozoic–Early Cenozoic plate tectonic framework of the Eastern Mediterranean. Surveys in Geophysics 8, 375–437.

Daly, L., Zinsser, H., 1973. Étude comparative des anisotropies de susceptibilité et d'aimantation rémanente isotherme: Conséquences pour l'analyse structurale et le paléomagnétisme. Annalle Géophysique 29, 189–200.

Day, R., Fuller, M.D., Schmidt, V.A., 1977. Hysteresis properties of

titanomagnetites: grain size and compositional dependence. Physics of the Earth and Planetary Interiors 13, 260–267.
Dewey, J.F., Pittman, W.C., Ryan, W.B.F., Bonnin, J., 1973. Plate tectonics and the evolution of the Alpine system. Geological Society of America Bulletin 84, 3137–3180.
Dilek, Y., Thy, P., Moores, E.M., Ramsden, T.W., 1990. Tectonic evolution of the Troodos ophiolite within the Tethyan framework. Tectonics 9, 811–823.
Dunlop, D.P., Özdemir, Ö., 1997. Rock Magnetism: Fundamentals and Frontiers. Cambridge University Press, Cambridge.
Eaton, S., Robertson, A.H.F., 1993. The Miocene Pakhna Formation, southern Cyprus and its relationship to the Neogene tectonic evolution of the Eastern Mediterranean. Sedimentary Geology 86, 273–296.
Flinn, D., 1965. On the symmetry principle and the deformation ellipsoid. Geological Magazine 102, 36–45.
Grand, T., Lapierre, H., Mascle, G.H., Ohnenstetter, M., Angelier, J., 1993. Superimposed tectonics of the Cyprus ophiolitic massifs. Tectonics 12, 93–101.
Henry, B., 1983. Interprétation quantitative de l'anisotrophie de susceptibilitié magnétique. Tectonophysics 91, 165–177.
Housen, B.A., van der Pluijm, B.A., 1990. Chlorite control of correlations between strain and anisotropy of magnetic susceptibility. Physics of the Earth and Planetary Interiors 61, 315–323.
Housen, B.A., van der Pluijm, B.A., 1991. Slaty cleavage development and magnetic anisotropy fabrics. Journal of Geophysical Research 96, 9937–9946.
Housen, B.A., Richter, C., van der Pluijm, B.A., 1993a. Composite magnetic anisotropy fabrics: experiments, numerical models, and implications for the quantification of rock fabrics. Tectonophysics 220, 1–12.
Housen, B.A., van der Pluijm, B.A., van der Voo, R., 1993b. Magnetite dissolution and neocrystallization during cleavage formation: paleomagnetic study of the Martinsburg Formation, Lehigh Gap, Pennsylvania. Journal of Geophysical Research 98, 13799–13813.
Hrouda, F., 1986. The effect of quartz on the magnetic anisotropy of quartzite. Studia Geophysica et Geodetica 30, 39–45.
Jackson, M., 1991. Anisotropy of magnetic remanence: a brief review of mineralogical sources, physical origins, and geological applications and comparison with susceptibility anisotropy. Pure and Applied Geophysics 136, 1–28.
Jackson, M.J., Tauxe, L., 1991. Anisotropy of magnetic susceptibility and remanence: Developments in the characterization of tectonic, sedimentary, and igneous fabric. Reviews in Geophysics 29, 371–376.
Jelinek, V., 1981. Characterization of the magnetic fabric of rocks. Tectonophysics 79, 63–67.
Knopf, E.B., Ingerson, E., 1938. Structural Petrology. Geological Society of America Memoir 6, 270 pp.
Lapierre, H., Angelier, J., Cogné, X., Grand, T., Mascle, G., 1988. Tectonique superposée de la zone de faille d'Arakapas (Massif de Troodos, Chypre). Geodinamica Acta 2–4, 197–206.
McCabe, C., Jackson, M.J., Ellwood, B.B., 1985. Magnetic anisotropy in the Trenton limestone: Results of a new technique, anisotropy of anhysteretic susceptibility. Geophysical Research Letters 12, 333–336.
McCallum, J.E., Robertson, A.H.F., 1990. Pulsed uplift of the Troodos Massif—evidence from the Plio-Pleistocene Mesaoria basin. In: Malpas, J., Moores, E., Panayiotou, A., Xenophontos, C. (Eds.), Ophiolites: Oceanic Crustal Analogues, Proceedings of the Symposium 'Troodos 1987'. Cyprus Geological Survey Department, pp. 217–230.
Musaka, S.B., Ludden, J.N., 1987. Uranium–lead isotopic ages of plagiogranites from the Troodos ophiolite, Cyprus, and their tectonic significance. Geology 15, 825–828.
Orsag-Sperber, F., Rouchy, J.M., Elion, P., 1989. The sedimentary expression of regional tectonic event during the Miocene–Pliocene transition in the southern Cyprus basins. Geological Magazine 136, 291–299.
Payne, A.S., Robertson, A.H.F., 1995. Neogoene supra-subduction zone extension in the Polis graben system, west Cyprus. Journal of the Geological Society, London 152, 613–628.
Ramsay, J.G., 1967. Folding and Fracturing of Rocks. McGraw-Hill, New York.
Ramsay, J.G., Huber, M.I., 1983. The Techniques of Modern Structural Geology, Volume 1: Strain Analysis. Academic Press, Toronto.
Richter, C., van der Pluijm, B.A., 1993. Separation of paramagnetic and ferrimagnetic susceptibilities using low temperature magnetic susceptibilities and comparison with high field methods. Physics of the Earth and Planetary Interiors 82, 113–123.
Robertson, A.H.F., 1977. Tertiary uplift history of the Troodos massif, Cyprus. Geological Society of America Bulletin 88, 1763–1772.
Robertson, A.H.F., 1990. In: Malpas, J., Moores, E., Panayiotou, A., Xenophontos, C. (Eds.), Ophiolites: Oceanic Crustal Analogues, Proceedings of the Symposium 'Troodos 1987'. Cyprus Geological Survey Department, pp. 235–250.
Robertson, A.H.F., Woodcock, N.H., 1979. Mamonia Complex, southwest Cyprus: Evolution and emplacement of a Mesozoic continental margin. Geological Society of America Bulletin. Part I 90, 651–665.
Robertson, A.H.F., Woodcock, N.H., 1986. The role of the Kyrenia Range Lineament, Cyprus in the geological evolution of the Eastern Mediterranean area. Philosophical Transactions of the Royal Society of London A317, 141–177.
Rochette, P., 1987. Magnetic susceptibility of the rock matrix related to magnetic fabric studies. Journal of Structural Geology 9, 1015–1020.
Rochette, P., Fillion, G., 1988. Identification of multicomponent anisotropies in rocks using various field and temperature values in a cryogenic magnetometer. Physics of the Earth and Planetary Interiors 51, 379–386.
Rochette, P., Jackson, M., Aubourg, C., 1992. Rock magnetism and their interpretations of the anisotropy of magnetic susceptibility. Reviews in Geophysics 30, 209–226.
Rotstein, Y., 1984. Counterclockwise rotation of the Anatolian Block. Tectonophysics 108, 71–91.
Tarling, D.H., Hrouda, F., 1993. The Magnetic Anisotropy of Rocks. Chapman & Hall, New York.
Turner, F.J., Weiss, L.E., 1963. Structural Analysis of Metamorphic Tectonites. McGraw-Hill, New York.
Wasilewski, P.J., 1973. Magnetic hysteresis in natural materials. Earth and Planetary Science Letters 20, 67–72.
Werner, T., Borradaile, G.J., 1996. Paleoremanence dispersal across a transpressional Archean terrain: Deflection by anisotropy or by late compression? Journal of Geophysical Research 101, 5531–5545.
Woodcock, N.H., 1977. Specification of fabric shapes using an Eigenvalue method. Geological Society of America Bulletin 88, 1231–1236.